

Crater formation mechanism on the surface of a biaxially oriented polypropylene film

メタデータ	言語: eng 出版者: 公開日: 2017-10-03 キーワード (Ja): キーワード (En): 作成者: メールアドレス: 所属:
URL	http://hdl.handle.net/2297/32282

Study of the crater formation mechanism on the surface of BOPP film

Satoshi Tamura, Koichi Takino*, Toshiro Yamada*, Toshitaka Kanai**

E-mail: Satoshi1.Tamura@primepolymer.co.jp

Prime Polymer Co., Ltd., Kanazawa University*, Idemitsu Kosan Co., Ltd.**

580-30, Nagaura, Sodegaura-city, Chiba, 299-0265 JAPAN

Kakuma-machi, Kanazawa, Ishikawa, 920-1192 JAPAN*

1-1, Anesaki-Kaigan, Ichihara-city, Chiba, 299-0193 JAPAN**

Key words: films, orientation, poly(propylene) (PP), surfaces

Abstract

Biaxially oriented polypropylene (BOPP) films are used in a variety of areas around the world. They are especially suited for food packaging and industrial usages due to their high productivity. Many studies on stretchability regarding crystal structure changes have been reported by various researchers, since the machine speed has been increasing and the demand to produce thinner films has been becoming more important. Furthermore, a number of studies on the surface structure of BOPP films with crater-like roughness have been reported since the 1980's. Although the crater-like surface roughness was formed under specific film process conditions, the formation mechanism and the controlling method of the crater-like film surface are yet to be clarified. In this report, the authors demonstrate a new hypothesis as to the crater-like film surface roughness formation mechanism by analyzing the morphology of the surface layer of polypropylene (PP) sheets and by investigating the relationship between the surface structure changes and the entire structure changes. As a result, it was found that it needs to have over critical crystallization time in order to form the crater on the surface of BOPP film, and the crater formation mechanism was closely related not only to the surface structure changes but also to the deforming phenomenon of spherulite in PP sheet during stretching. Furthermore, this report will show the controlling factors in the formation of the crater structure from the view point of production conditions.

1. Introduction

PP is one of the most popular thermoplastic resins and is produced at a rate of about 42 million tons per year around the world ¹⁾. It is a well known fact that there are some crystal types of PP with different crystal systems, and surface roughness of BOPP films has been investigated in association with crystal types ²⁻⁸⁾. Many basic studies have been reported on the formation of α and β crystals ⁹⁻¹⁴⁾. Natta and Corradini reported in their report in 1960 that unit lattice of α crystal is the monoclinic system, and now it is known as being the most dominant crystal in PP ⁹⁾. β crystal was discovered by Keith in 1959, and the unit lattice is a hexagonal system ¹⁰⁾. It was reported that β crystals are formed easily by adding β nucleator into raw PP ¹¹⁾, under the controlled temperature gradient ¹²⁾, and under a strong shear stress in the extruder such as at a low extruding temperature ¹³⁾. In addition to these studies, the characteristics of β crystal were reported and it was found that they have lower densities and melting points than those of α crystal ⁹⁾.

It was also reported that the formation of crater-like surface roughness of BOPP films is due to the crystal dislocation system. Since β crystals with lower density change into α crystals with higher density after stretching the sheets which contain both α and β crystals, the craters were formed where the β crystals existed. In order to obtain the crater-like surface roughness of BOPP films, Fujiyama et al. reported that the stretching temperature in the machine direction (MD) process should be controlled between the melting points of both β and α crystal ³⁾. It was also reported that the stretching temperature in the transverse direction (TD) process should be controlled between 150°C and 155°C, because the craters became unclear in roughened BOPP film at a temperature lower than 150°C and the craters disappeared by melting at a temperature higher than 155°C ⁴⁾. On the other hand, although Fujiyama et al. reported that the difference of the surface roughness between the BOPP film produced by the sheet with α nucleator and that with β nucleator, the relationship between the crater shape and β crystals with regard to parameters such as amount and shape has not yet been clarified ⁵⁾. It was reported that there was a good relationship between the chill-roll temperature and the average roughness Ra of BOPP film surface which is a parameter of crater depth, but the relationship between the chill-roll temperature and crater diameter is yet not clear ⁶⁾. From these reports, the crater formation mechanism of BOPP films has not yet been clarified, because these reports only focused on the β crystals.

Various studies have reported on the change of the crystal structure during the stretching process ¹⁵⁻²³. Although Koike et al. made a report on the change of PP crystal structure during the uniaxial stretching observed by the birefringence technique ¹⁵) and Phillips et al. made a report on the relationship between the stretching stress and the change of morphology of the PP sheet ¹⁶), no information related to the surface structure was reported. Kanai et al. reported on the PP spherulites deformation and crystalline orientation during stretching in terms of the stretching stress pattern, and on the analytical results of the crystal structure changes observed by birefringence, light scattering and small-angle X-ray scattering (SAXS) ¹⁷⁻²⁰). Kanai et al. also reported that there was a strong relationship between the observation results of crystal structures in PP sheets and the simulation results obtained by cooling calculations conducted with regard to the thermal transfer characteristics of PP sheets using the chill-roll cooling system ²¹⁻²³). Although it was concluded in the report that the cooling simulation is an efficient method to control the crystallization of a PP sheet which is an important factor of stretchability of BOPP, there was no information on the surface structure of BOPP.

It was found in our previous report ²⁴) that the crater-like structures on BOPP film surface were related to the morphology of the surface layer of the PP sheets. However, even though it is an important factor in the formation when discussing the crater-like structure of BOPP, the method to control the morphology of the PP sheet has not yet been discussed. The relationship between the changes of the surface structure and the whole structure has not yet been discussed either. Therefore, this report will give some perspective on the formation mechanism of craters with regard to controlling the morphology of the surface layer of PP sheet and also on its connection to changes in the entire structure.

2. Experiments

1) Samples

In order to clarify the mechanism for the formation of the surface craters, PP-A of a high tacticity with a meso pentad mmmm value of 96mol% which is a parameter of the isotactic index measured by ¹³C-NMR was prepared. Thermal properties of melting point (T_m), melting enthalpy (ΔH_m), and crystallization temperature (T_c) were measured by differential scanning calorimetry (DSC, PerkinElmer B014-3018/B014-3003), and the

molecular weight distribution parameter M_w/M_n was measured by gel permeation chromatography (GPC). Properties of PP-A are shown in Table 1.

PP sheets were produced using a sheet forming machine (GM Engineering) with a diameter of 35mm extruder (Fig.1). The PP resin was extruded from a T-die with a width of 200mm at 250°C. It was cast by a chill-roll with a diameter of 250mm at a speed of 0.8 m/min and PP sheets with various thicknesses were produced at various chill-roll temperatures in order to investigate the relationship between the morphology of PP sheet and the sheet forming conditions. In this report, samples were named in order of resin type, chill-roll temperature, and thickness. For example, a sample 'A80-500' is the sheet made by PP-A at a chill-roll temperature of 80°C with a thickness of 500µm. The BOPP film names were defined by putting 'f' at the end of PP sheet names, for example 'A80-500f'.

Fig.2 shows the schematic diagram for the production and evaluation methods of sample. After PP sheets were cut into a square shape of 85 × 85mm in size, they were stretched to BOPP films by a table tenter (Bruckner KARO IV) in order to analyze the surface structure. After they were preheated at a definite temperature for 1 minute, it was stretched at maximum stretching ratios of 5 times to the machine direction (MD) at first, and next 7 times to the transverse direction (TD). PP sheets were also stretched by the opt-rheometer (Orc Manufacturing Co., Ltd.) in order to analyze the crystal structure changes. PP sheets with a rectangular shape of 25 × 10mm were stretched to the MD at a stretching ratio of 5 times at a strain speed of 28.6 %/s after preheating at 159°C for 5 minutes. The stretching force was measured by a load cell which was equipped on a chuck of the opt-rheometer with maximum load of 100N.

2) Evaluation of PP sheets and the BOPP films

Analyzing methods of PP sheets and BOPP films and the properties obtained from these measurements were shown in Table 2. The sectional structures of PP sheets were observed by an optical microscope (Nikon ECLIPSE-LV100POL). On observing morphologies of the PP sheet of sectional view using an optical microscope, crystal sizes were measured by visual inspection from pictures taken with a polarizing lens. Thermal properties of T_m and ΔH_m of PP sheets were measured by DSC (PerkinElmer B014-3018/B014-3003) at a heating

rate of 10°C/min.

X-ray diffractions were measured on the PP sheets with a Rigaku Denki RINT-2500 diffractometer with Ni-filtered Cu-K α radiation. The crystallinity χ_c and the β crystal content named as the K-value of PP sheets were calculated from the X-ray diffraction curves^{25, 26}. The change of the crystal structure during stretching was analyzed by light scattering data obtained by the opt-rheometer using a high power He-Ne laser. Spherulite size U_{max} of PP sheet was calculated from equation (1) obtained by the Hv scattering pattern which reflects the scattering of the polymer superstructure

$$U_{max} = \frac{4.09}{(4\pi/\lambda) \sin\theta_{max}} \quad \cdot \cdot \cdot \cdot \cdot \quad (1)$$

where λ is the wavelength of He-Ne laser (632.8nm), and θ_{max} is the scattering angle which indicates the yield point of scattering intensity to 45° against a plane of polarization, respectively.

The surface structures of BOPP films were observed by Scanning Electron Microscope (SEM, JOEL JSM5600LV). Samples were sputtered with gold in a vacuumed atmosphere and the crater diameters were measured by visual inspection from photographs. In addition, the shapes of the craters were measured by a highly precise shape measuring machine (Kosaka Laboratory SURFCODER ET4000A) using a diamond head at a head pressure of 70 μ N. Ten points average roughness Rz defined by JIS B0601 [1994] was used as the parameter of depth of crater on BOPP films surface.

Moreover, in order to investigate the crater formation mechanism at the surface layer of PP sheet, the influence of cooling speed was studied at the sheet forming condition described at section 2.1). The temperature of PP resin starts to drop after PP sheet is extruded from the die and touches the chill-roll. PP crystallization starts when the sheet temperature reaches the crystallization temperature, at 115°C in the case of PP-A. After sheet temperature is kept at the crystallization temperature until the latent heat ΔH is consumed, the sheet temperature starts to drop again. Crystallization time is defined as the time during which PP sheet temperature is kept at the crystallization temperature, and PP crystallizes during the crystallization time. In this report, it is assumed that heat is conducted by primary thermal conduction expressed in equation (2) and is transferred at the

boundary condition expressed in equation (3).

$$\frac{\partial T}{\partial t} = \frac{k}{C_p \cdot \rho} \cdot \frac{\partial^2 T}{\partial x^2} \quad \dots \dots \dots (2)$$

$$k \frac{\partial T}{\partial x} = h (T_w - T_\infty) \quad \dots \dots \dots (3)$$

where T is sheet temperature (K), t is time (s), k is thermal conductivity (0.28W/m·K), C_p is heat capacity (1.93 J/kg·K), ρ is density of PP, x is sheet position from chill-roll (m), h is heat-transfer coefficient (756W/m²·K), T_w is surface temperature of sheet (K), and T_∞ is chill-roll temperature (K), respectively. Although the density ρ of PP depends on temperature, the fixed value 890kg/m³ was used in this study in order to make the calculation simple. Heat-transfer coefficient h was determined by measuring the real temperature of chill-roll and PP sheet using a touched type thermometer.

3. Results and Discussion

1) The influence of sheet forming conditions on the crater formation of BOPP film

First, the influence of thickness of PP sheets on the crater structure was studied. Fig.3 shows the polarized micrographs of the cross-sectional views of PP sheets in the MD and normal direction (ND). As for A80-500 sheet, a number of white grains are observed only in the surface layer of the opposite side of chill-roll. Since the amorphous parts are not portrayed in white on a polarizing microscope, these white grains are considered to be β crystals of PP⁴⁾ and also trans-crystals^{27, 28)}. Although these white crystal grains were observed even in the A80-400 and A80-300 sheets with thicknesses of 400 and 300μm, they were not observed in the A80-200 and A80-100 sheets with thicknesses of 200 and 100μm, respectively. Fig.4 shows the relationship between shapes of crystal structure and thickness of PP sheet. As a result, although the crystal grains were not observed in the surface layer of chill-roll side, the crystal grains size (depth and diameter) in the surface layer of the opposite side of chill-roll became larger as the PP sheet became thicker than 200μm. Whereas the size of spherulite in the center

of PP sheet got larger as the PP sheet became thicker from 100 μm .

In order to discuss more deeply, PP sheet was analyzed by DSC and WAXD. T_m gradually increased from 164.5 $^{\circ}\text{C}$ to 167.7 $^{\circ}\text{C}$ as PP sheet thickened (Fig.5 (a)). Since T_m is closely related to the thickness of lamella²⁹⁾, the result indicates that lamella becomes thicker with the increase of PP sheet thickness. ΔH_m slightly increased as the thickness of PP sheet increased from 100 μm to 300 μm and saturated from 300 μm to 500 μm (Fig.5 (a)), agreeing with the behavior of crystallinity χ_c measured by WAXD (Fig.5 (b)). Furthermore, β crystal was detected at the thickness of PP sheet of 400 μm or more.

Next, the surface structures of BOPP films obtained by stretching PP sheets with different thicknesses were observed (Fig.6). Clear crater structures were observed on the opposite side of the chill-roll of BOPP films obtained from the PP sheets with thicknesses from 500 to 300 μm . Crater structures were not observed on BOPP films obtained from A80-200 and A80-100 sheets, or on the chill-roll side of all the samples. These results show an adequate relationship between the existences of the crystal grains on the PP sheets and the formation of craters on BOPP films. Fig.7 shows the relationship between the crater shape and thickness of PP sheets. Crater shape indicated an adequate relationship with the thickness of PP sheet. Fig.8 shows the relationship between the crystal grain structure of PP sheets and the crater structure of BOPP films. Since there was also a good relationship between the crystal grain structure and crater structure, it is assumed that the formation mechanism of crater is related to the crystal deformation.

These results indicate that crater shape can be controlled by the white crystal grains size which is influenced by the thickness of PP sheet. In order to discuss more deeply, sheet temperatures at several distances from the surface of the opposite side of chill-roll were simulated by equation (2) and (3). Fig.9 (a) shows the calculated results of A80-500 at the intervals of 100 μm , 0 μm means the surface of the opposite side of chill-roll and 500 μm means the surface of chill-roll side. From these results, we can see that the temperature of the chill-roll side drops faster than that of the opposite side of chill-roll. In order to investigate the influence of the thickness of PP sheet on the sheet surface temperature, calculated results of the primary sheet temperatures of the opposite side of chill-roll and chill-roll side are shown in Fig.9 (b) and (c), respectively. The flat area at a crystallization temperature of 115 $^{\circ}\text{C}$ was observed by the opposite side of chill-roll of A80-500, but no flat area

was observed on both sides of A80-100. These flat areas from 106°C to 124°C were defined as the crystallization time, and the relationship between the calculated results of crystallization time and crystal grain sizes are shown in Fig.9 (d). As a result, it was found that there was an adequate relationship between them. Furthermore, the relationship between the crystallization time and the crater formation was investigated (Fig.9 (e)). From these results, it was found that more than 1.5 seconds for the crystallization time is required in order to create the crystal grain and crater on BOPP films on the opposite side of chill-roll at our experimental method, and this study with regard to the thickness of PP sheet has not been discussed in the previous reports.

Next, the influence of the chill-roll temperature on the crater structure was studied. Fig.10 shows the polarized micrographs of the cross-sectional views of PP sheets at the MD and ND. Crystal grains were not observed in the surface layer of both side of the chill-roll with the chill-roll temperatures ranging from 30°C to 65°C. On the other hand, a lot of crystal grains in the surface layer of the opposite side of the chill-roll from A80-300 to A95-300 sheets with chill-roll temperatures from 80 to 95°C were formed, and they became larger with the increase of the chill-roll temperature (Fig.11). Furthermore, crystal grains in the surface layer of the chill-roll side were observed with the chill-roll temperature at and above 90°C, although they were not observed in the surface layer of A80 sheets cast at 80°C with several thicknesses from 500 to 100µm.

Fig.12 shows the melting properties and crystal structures measured by DSC and WAXD. Since T_m and ΔH_m increased as the chill-roll temperature increased, it is assumed that the thickness of lamella and the amount of crystal part will increase with the increase of chill-roll temperature, or in other words, with cooling slowly (Fig.12 (a)). As a proof, crystallinity χ_c increased with the increase of chill-roll temperature (Fig.12 (b)). Furthermore, β crystal was detected at and above the chill-roll temperature of 90°C.

Fig.13 shows the SEM images of the surface of BOPP films obtained from PP sheets with different chill-roll temperatures. Although crater structures were not observed on the surface of the opposite side of chill-roll from A30-300f to A65-300f films, they were observed from A80-300f to A95-300f films. Additionally, they were observed on the surface of the chill-roll side too from A90-300f and A95-300f in which crystal grains in the surface layer of the chill-roll side were observed in the PP sheets. From these results, a higher chill-roll temperature is required to produce craters on the BOPP film surface of chill-roll side. Furthermore, crystal grains

in PP sheet are needed in order to produce craters on BOPP film.

In order to investigate the influence of the chill-roll temperature on the sheet surface temperature, calculated results of the primary sheet temperatures of the opposite side of chill-roll and chill-roll side are shown in Fig.14 (a) and (b), respectively. The crystallization time became longer as the chill-roll temperature became higher. This graph shows that a crystallization time of more than 1.5 seconds is needed to create the crater on the surface of BOPP film at our experimental method. This result obtained from the PP sheet with the different chill-roll temperatures is similar to that of PP sheets of different thicknesses. It was confirmed that crater formation can be controlled by the crystallization time which is a function of the thickness of PP sheet and chill-roll temperature. In addition, craters can be formed on the BOPP film surface of the chill-roll side with controlling the crystallization time suitably, while the previous reports discussed only the cases of the crater on the surface of opposite side of chill-roll.

2) The relationship between the surface structure and the whole structure of BOPP film

In order to study the crater formation mechanism, PP sheets cast by different chill-roll temperatures of A80-300 with high crystallinity of 65% and A30-300 with low crystallinity of 34% measured by WAXD were stretched by an opt-rheometer which gives the information of superstructure during stretching. Fig.15 shows the change of the surface roughness parameter Rz value with the stretching ratio. Although Rz of A80-300 was larger than that of A30-300, Rz of both samples had a yield point at a stretching ratio of 2 times, and Rz gradually decreased as the stretching ratio increased. The reason for this is because the deep dent which is obtained at the early stage of the stretching process changed to a shallow crater with cutting through a thick wall at stretching ratios of 2 times or higher as was mentioned in our previous report²⁴⁾. In another word, despite the crystal grains are formed in the surface layer uniformly, the deformation of surface structure starts partially as the weak parts were stretched first. These results coincide with the results obtained by the stretching test using the table tenter and are assumed to be caused by the difference of crystal grains size between the sheets.

Fig.16 shows the change of light scattering pattern with the stretching ratio. A80-100 was used instead of A80-300 because the light scattering peak of A80-300 was too weak to analyze the data. The light scattering

patterns of un-stretched sheets of both samples show clear clover patterns which demonstrate the existence of spherulites. There were no considerable changes in the light scattering pattern at a stretching ratio of 2 times, and the spherulites still remained in the PP sheet (Table 3). Spherulites were destroyed at higher stretching ratios, because the clover pattern changed to a streak pattern to the equatorial direction. This result indicates that partial deformation of spherulite is observed at the stretching ratio lower than 2 times, and crystal structure changes totally at higher stretching ratios. Although the sizes of crystal grains of these two PP sheets were different, the deformation patterns of spherulites were similar in these two PP sheets. Since the stretching ratio with the maximum of Rz value and that of the existence limit of spherulite was the same, it is concluded that crater formation on BOPP films surface is closely related to the spherulite deformation of the entire BOPP films.

4. Conclusion

The formation mechanism of the crater-like surface roughness of BOPP film has been investigated. It was found that the thickness of PP sheet has a great effect on the crater shape of BOPP film because the crystal grains in the surface layer of PP sheet change accordingly to the thickness of PP sheets. The formation mechanism of the crater-like surface roughness of BOPP film has been investigated. It showed that crystallization time over a critical value is required to produce crystal grains in the surface layer of PP sheet with β type trans-crystals.

Furthermore, the effect of chill-roll temperature at the proceeding of PP sheet was investigated. It was found that the crystal grains in the surface layer are easily created at higher chill-roll temperature. From the analysis of the cooling calculation, it is confirmed that more than 1.5 seconds of the crystallization time is required to produce crystal grains in the surface regions of PP sheet. It was also found that crater could be formed on the both surfaces of BOPP films, irrespective of the sides of chill-roll, when the crystallization time was controlled for more than 1.5 seconds. It may be said that the technology of crater formation can be settled by the simulation of PP sheets produced by different conditions.

In addition, the crater formation mechanism was researched in terms of the stretching behavior of entire PP sheets using the opt-rheometer. The change of surface roughness with the stretching ratio showed that the

deformation of surface structure starts partially before the craters were formed on the BOPP films surface and Rz indicated maximum value at the stretching ratio of 2 times. In addition, it was found that spherulites began to destroy at the stretching ratio higher than 2 times by analyzing the light scattering method. As a result, it is concluded that crater formation on BOPP films surface is closely related to the spherulite deformation and collapse of the entire BOPP films.

5. References

- 1) Kagaku-Keizai, 3, 92-95(2011)
- 2) Fujiyama M., Kawamura Y., Wakino T., Okamoto T., J. Appl. Polym. Sci. 36, 985(1988)
- 3) Fujiyama M., Kawamura Y., Wakino T., Okamoto T., J. Appl. Polym. Sci. 36, 995(1988)
- 4) Fujiyama M., Kawamura Y., Wakino T., Okamoto T., J. Appl. Polym. Sci. 36, 1011(1988)
- 5) Fujiyama M., Kawamura Y., Wakino T., Okamoto T., J. Appl. Polym. Sci. 36, 1025(1988)
- 6) Fujiyama M., Kawamura Y., Wakino T., Okamoto T., J. Appl. Polym. Sci. 36, 1035(1988)
- 7) Fujiyama M., Kawamura Y., Wakino T., Okamoto T., J. Appl. Polym. Sci. 36, 1049(1988)
- 8) Fujiyama M., Kawamura Y., Wakino T., Okamoto T., J. Appl. Polym. Sci. 36, 1061(1988)
- 9) G. Natta, P. Gorradini, Nuovo Cimento Suppl., 15, 40(1960)
- 10) Keith H. D., Padden F. J., Walter N. M., Wickoff H. W. J., Appl. Phys., 30, 1485(1959)
- 11) Asano T., Fujiwara Y., Polym. J., 11, 383(1979)
- 12) Meille S. V., Ferro D. R., Bruckner S., Lovinger A. J., Padden F. J., Macromolecules, 27,2615(1994)
- 13) Moitzi J., Skalicky P., Polymer, 34, 3168(1993)
- 14) Farah M., Bretas R., J. Appl. Polym. Sci. 91, 3528(2004)
- 15) Koike Y., and Cakmak M., Polymer 44, 4249-4260(2003)
- 16) Phillips R. A., and NGUYEN T., J. Appl. Polym. Sci. 80, 2400-2415(2001)
- 17) Sakauchi K., Uehara H., Yamada T., Obata Y., Takebe T., Kanai T. Polymer Processing Society Annual Meeting-21(2005)
- 18) Kanai T., Matsuzawa N., Takebe T., Yamada T., Polymer Processing Society Regional Meeting Europe

CD-ROM Abstracts(2007)

- 19) Kanai T., Matsuzawa N., Yamaguchi H., Takebe T., Yamada T. 24th Polymer Processing Society Annual Meeting CD-ROM Abstracts(2008)
- 20) Kanai T., Takebe T., Matsuzawa N., Yamaguchi H. Asian Workshop on Polymer Processing Plenary Lecture(2009)
- 21) Kanai T., Yonekawa F., and Kuramoto I 17th Polym. Proc. Society Annual Meeting Abstracts, 17(2001)
- 22) Kanai T., Seikei-Kakou, 18(1), 53-66(2006)
- 23) Matsuzawa N., Kamatani Y., Kanai T., Yamada T., Sakauchi K., Uehara H., 22th Polymer Processing Society Annual Meeting CD-ROM Abstracts(2006)
- 24) Tamura S., Ohta K., Kanai T., J. Appl. Polym. Sci., published on line, November 3rd (2011)
- 25) Natta G., Corradini P., Cesari M., Rend.Accad.Naz.Lincei, 22, 11(1957)
- 26) Tuner-Jones A., Aizilewood J. M., Beckert D. R., Makromol. Chem., 75, 134(1964)
- 27) Yamakita T., T. IEE. Japan, 117-A, 12(1997)
- 28) Bailey G. W., J. Polym. Sci., 62, 241(1962)
- 29) Layritzen J. I., Hoffman J. D., J. Res. Nat. Bur. Std., 64(a),73(1960)

Table 1 Properties of PP resin

Properties	Unit	PP-A
MFR	g/10min	3.5
mmmm	mol%	96
T _m	°C	164
ΔH _m	J/g	105
T _c	°C	115
M _w /M _n	-	5.1

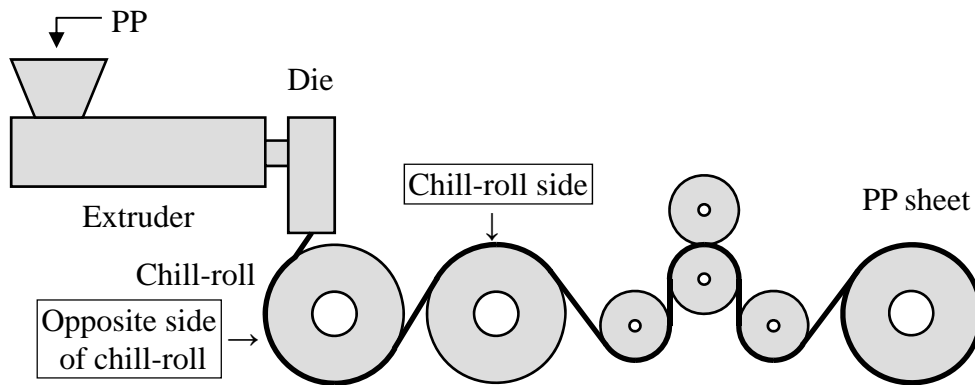


Fig. 1 Schematic diagram of PP sheet forming machine

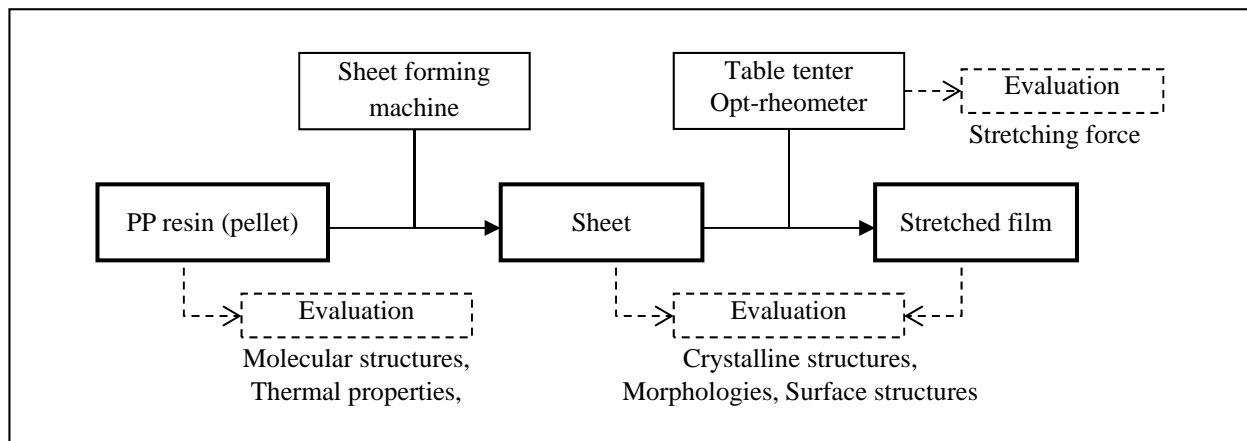


Fig. 2 Diagram production and evaluation methods of each sample

Table 2 Analyzing methods of PP sheets and films

Samples	Analyzing methods	Properties obtained from measurements
Sheets	OM DSC WAXD Light scattering	Sectional structures (size of crystal grain and spherulite) Thermal properties (T_m , ΔH_m) Crystalline structures (χ_c , K) Crystalline structures (U_{max})
Films	SEM Shape measuring machine	Crater shape (Diameter) Crater shape (Depth : Surface roughness (Rz))

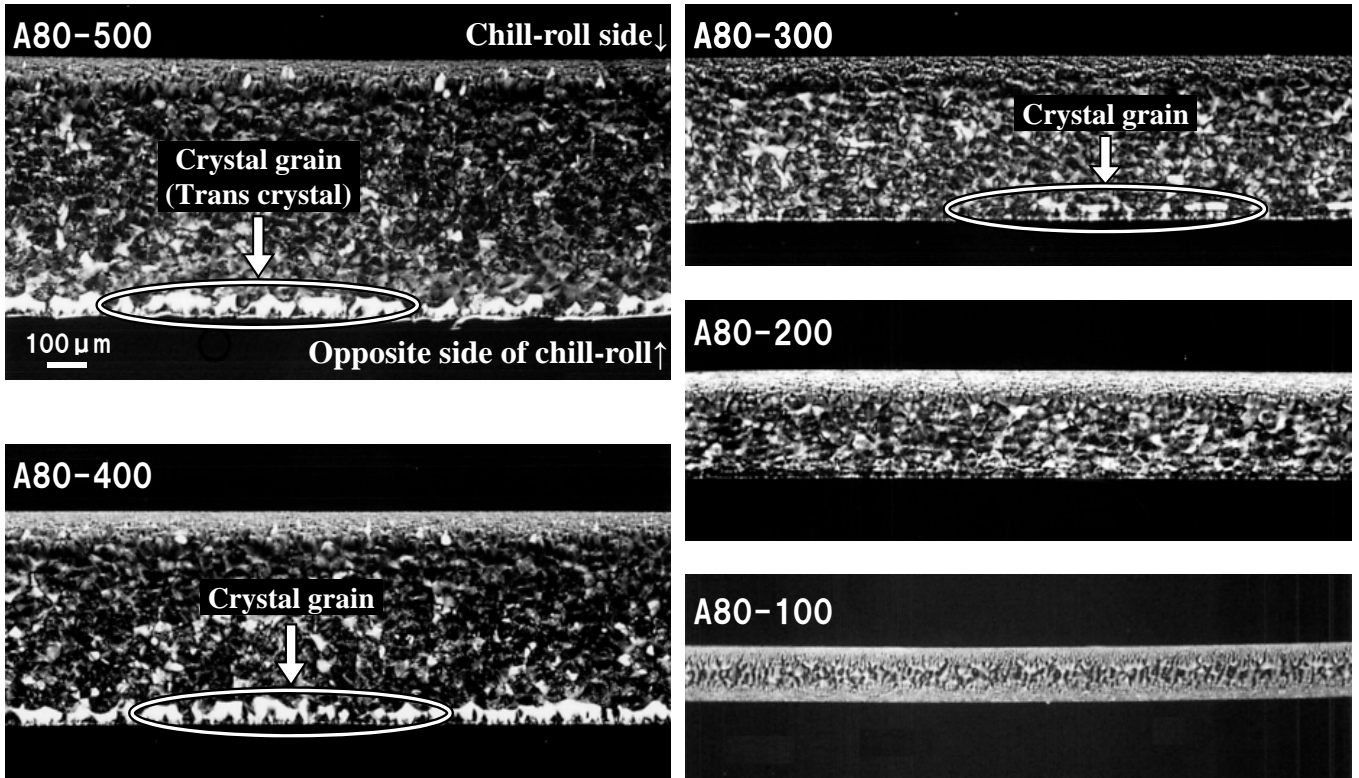


Fig.3 Optical microscope images of PP sheets with different thicknesses

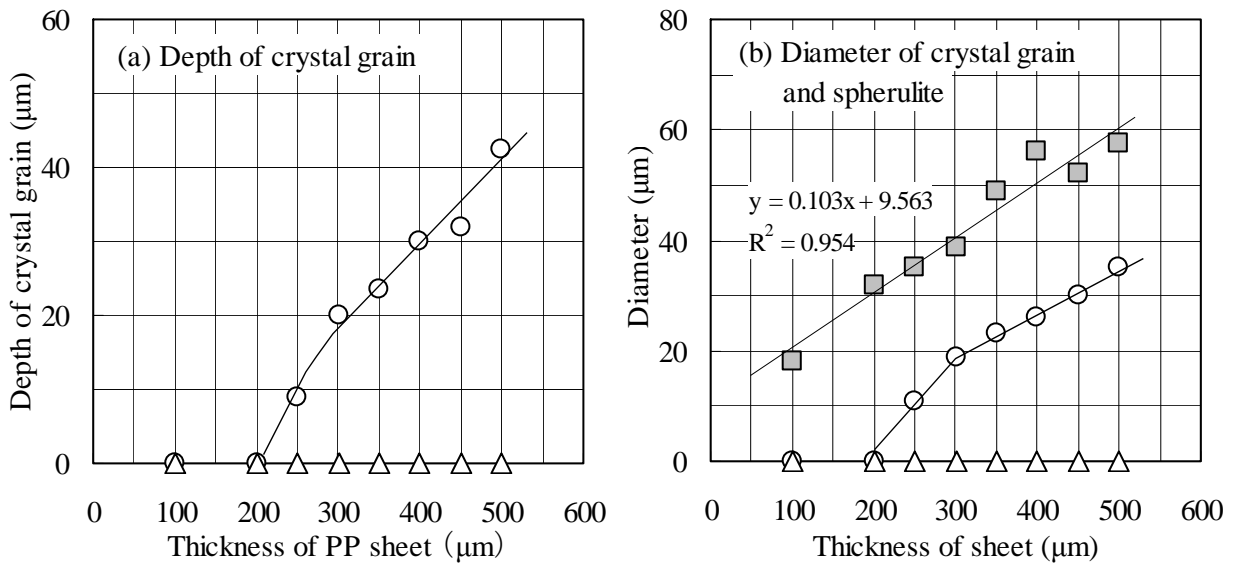


Fig. 4 Crystal structure of PP sheets with different thicknesses

- Crystal grain on the surface layer of opposite side of chill-roll
- △ Crystal grain on the surface layer of chill-roll side
- Spherulite in the central part of the sheet

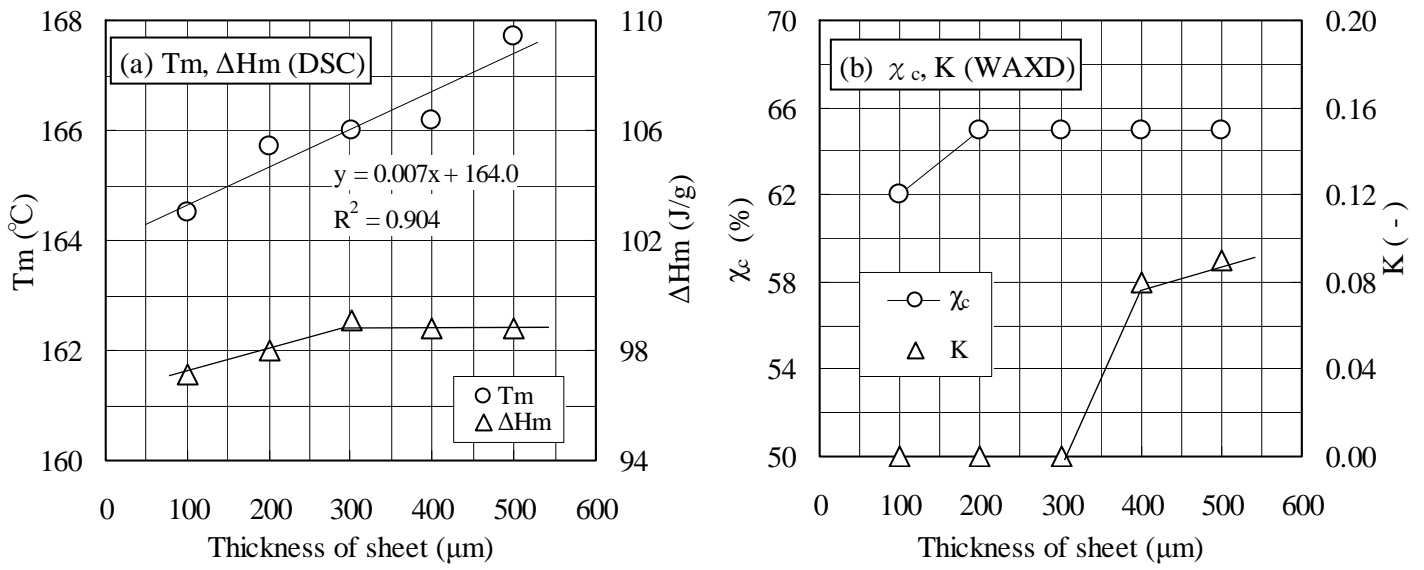


Fig.5 Properties of PP sheets with different thicknesses measured by (a) DSC and (b) WAXD

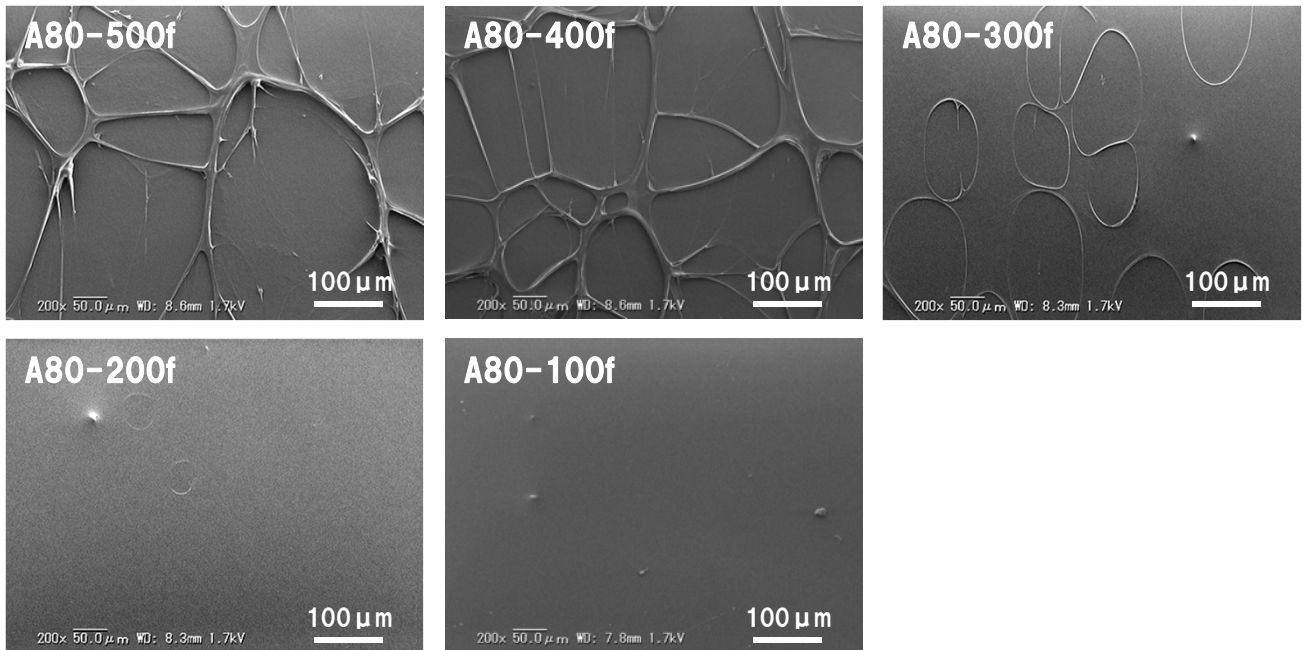


Fig.6 SEM images of BOPP films surface of opposite side of chill-roll, obtained from PP sheets with different thicknesses

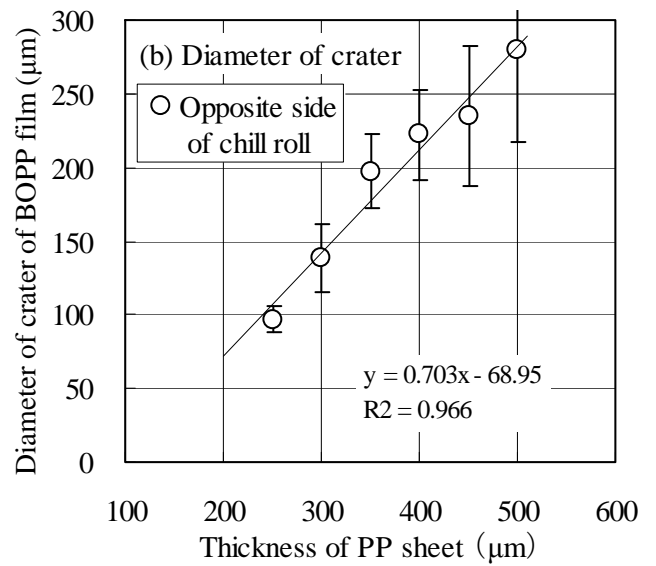
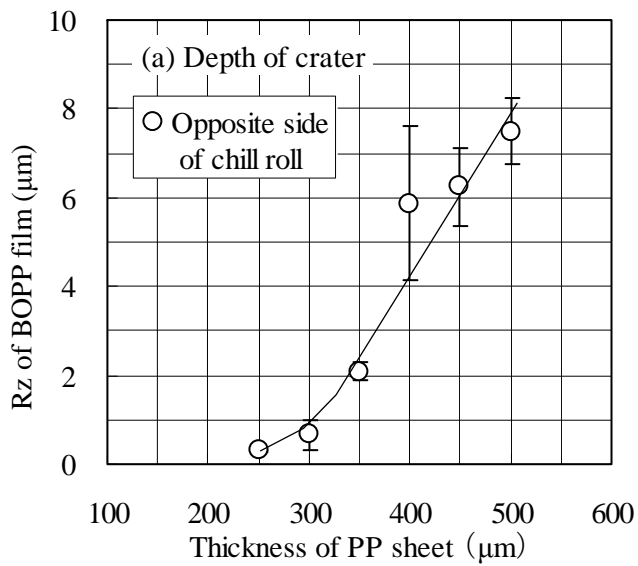


Fig.7 The relationship between PP sheet thickness and crater shape

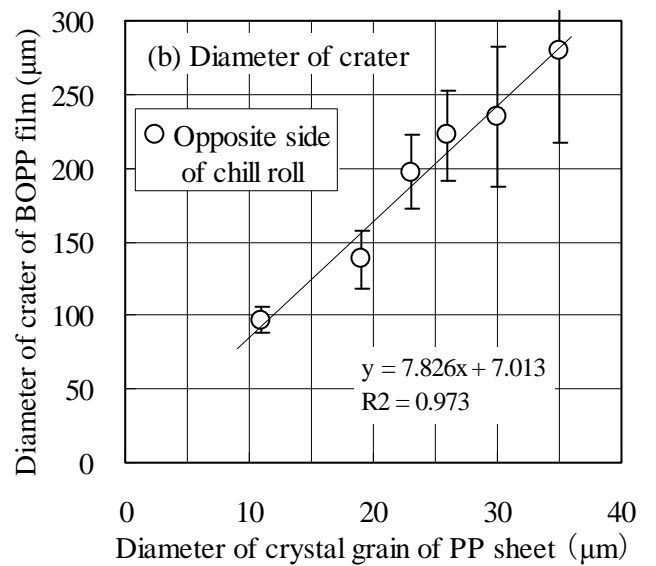
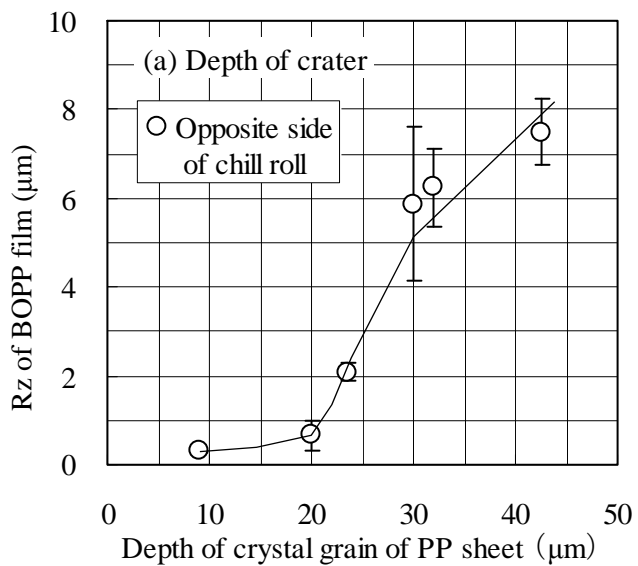


Fig.8 The relationship between crystal structure of PP sheets and crater structure of BOPP films

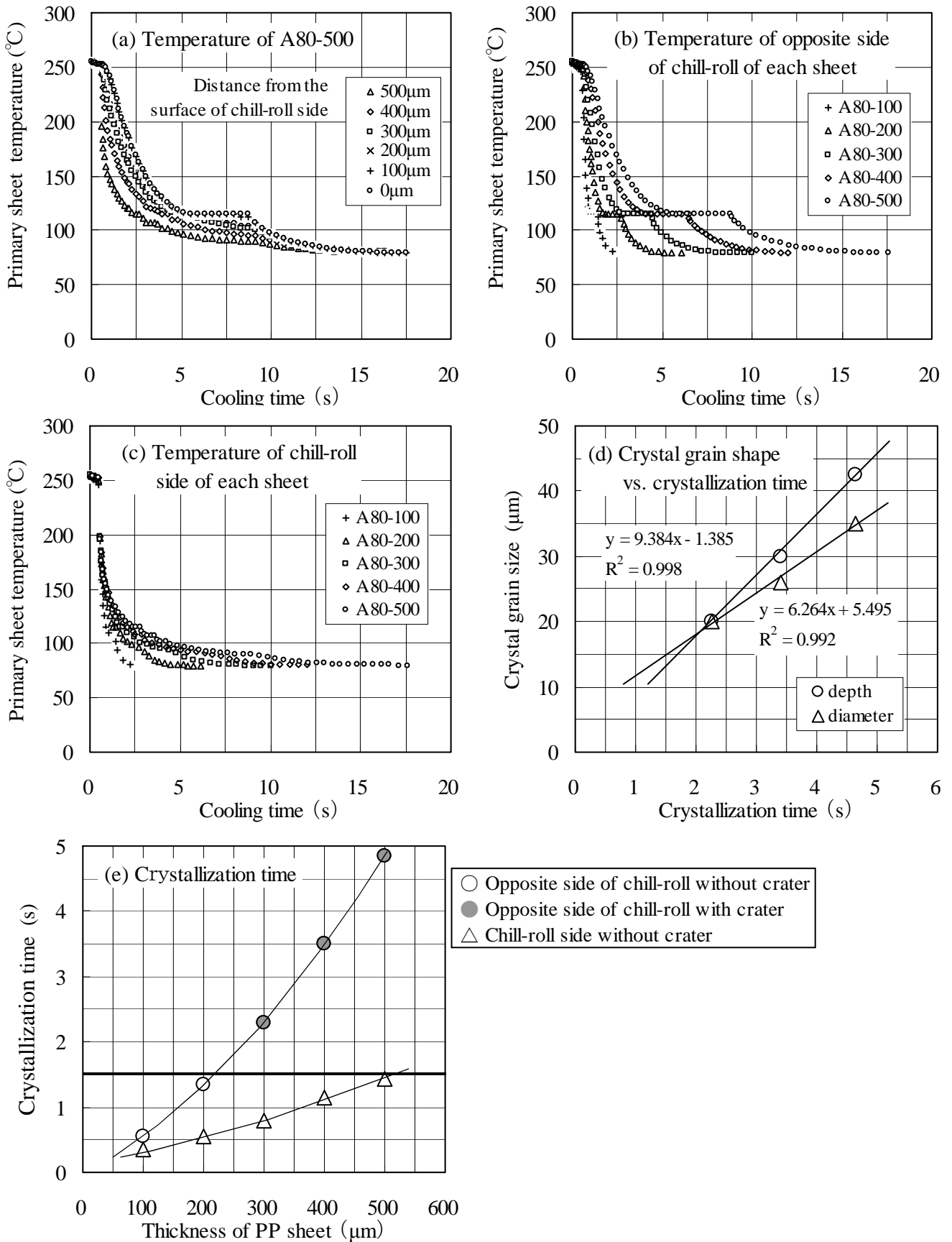


Fig.9 Calculated results of temperature of PP sheets with different thicknesses
 (Conditions: Die temperature; 250°C, Chill-roll temperature; 80°C,
 Stretching temperature; 159°C, Stretching ratio; MD/TD=5/7)

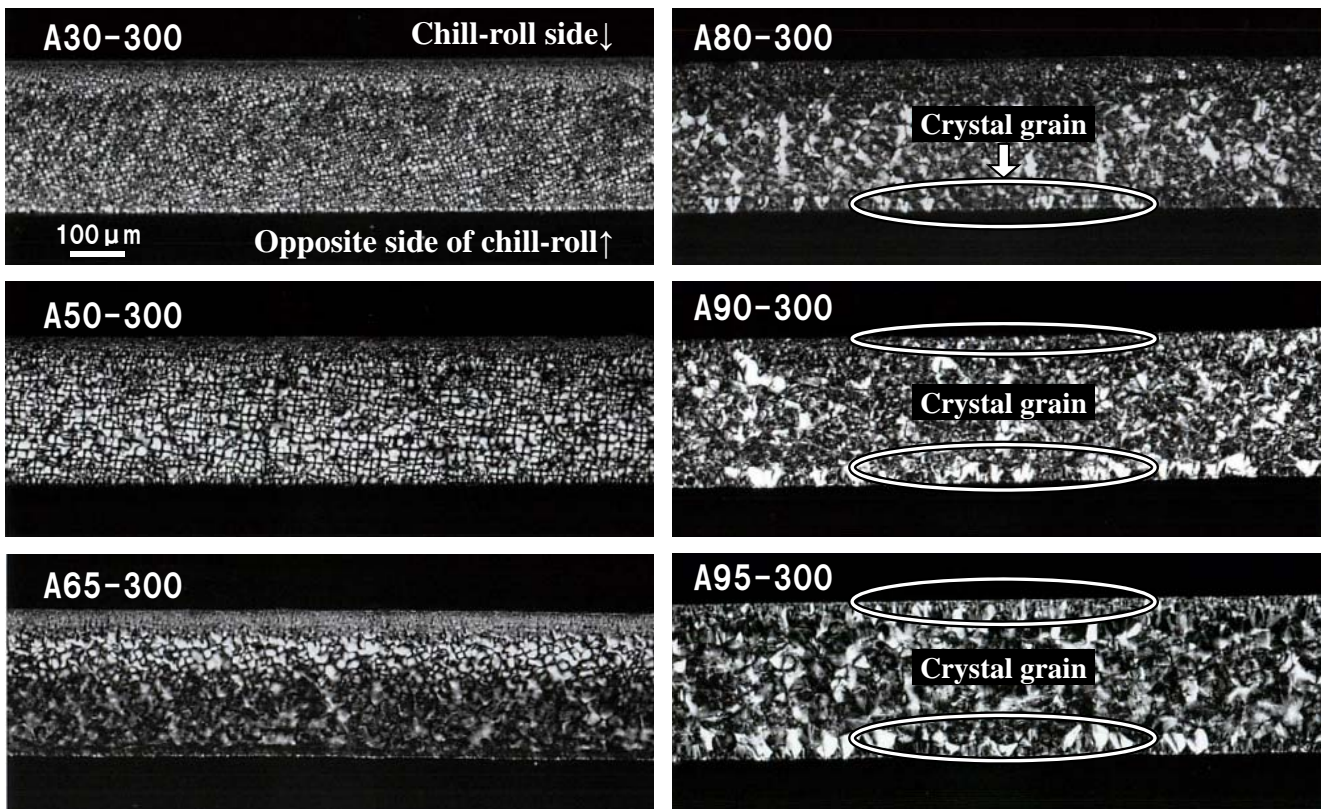


Fig.10 Optical microscope images of PP sheets with different chill-roll temperatures

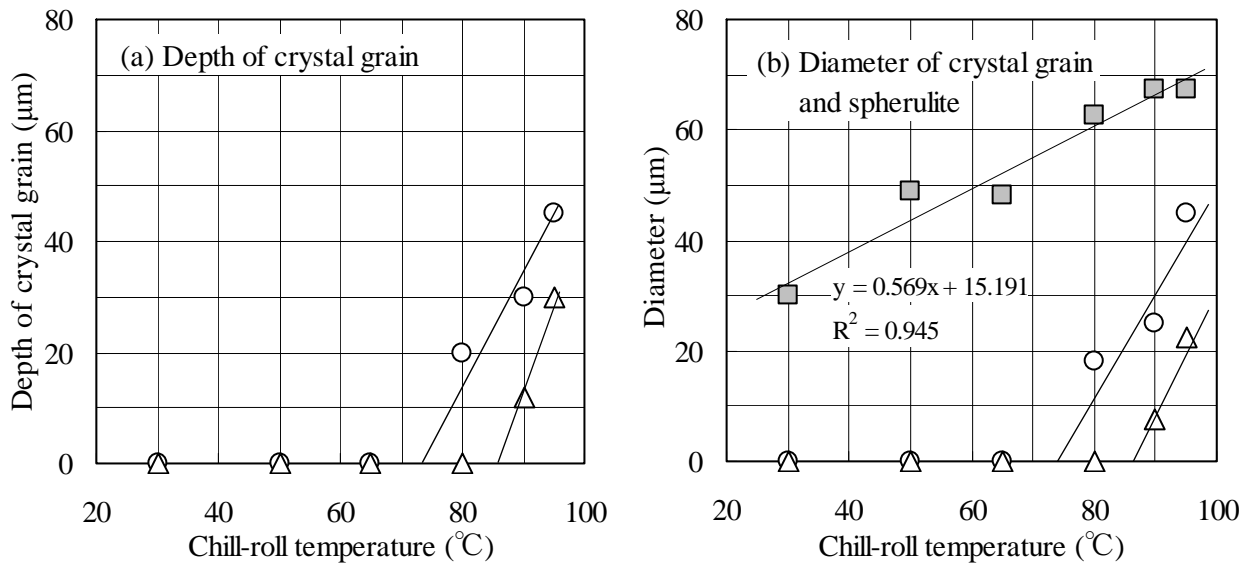


Fig.11 Crystal structure of PP sheets with different chill-roll temperatures

- Crystal grain on the surface layer of opposite side of chill-roll
- △ Crystal grain on the surface layer of chill-roll side
- Spherulite in the central part of the sheet

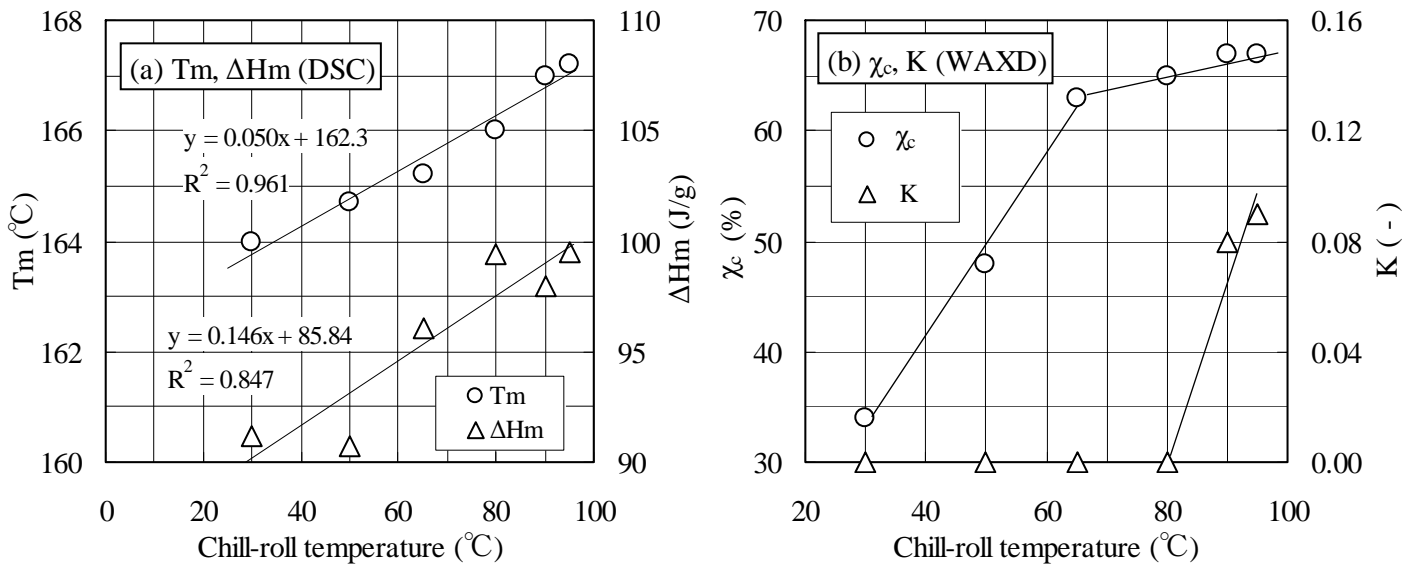


Fig.12 Properties of PP sheets with different chill-roll temperatures measured by (a) DSC and (b) WAXD

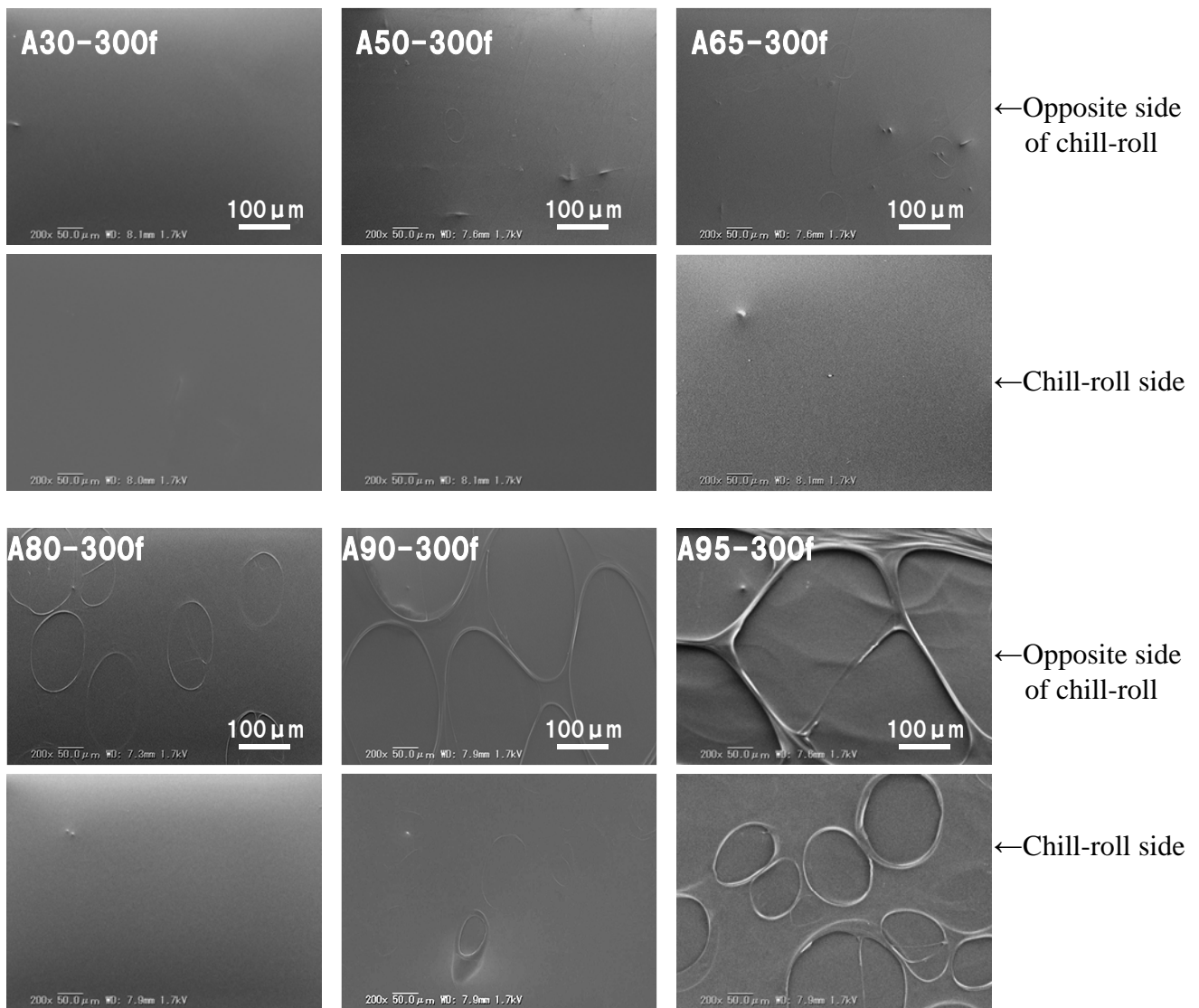


Fig.13 SEM images of BOPP films surface obtained from PP sheets with different chill-roll temperatures

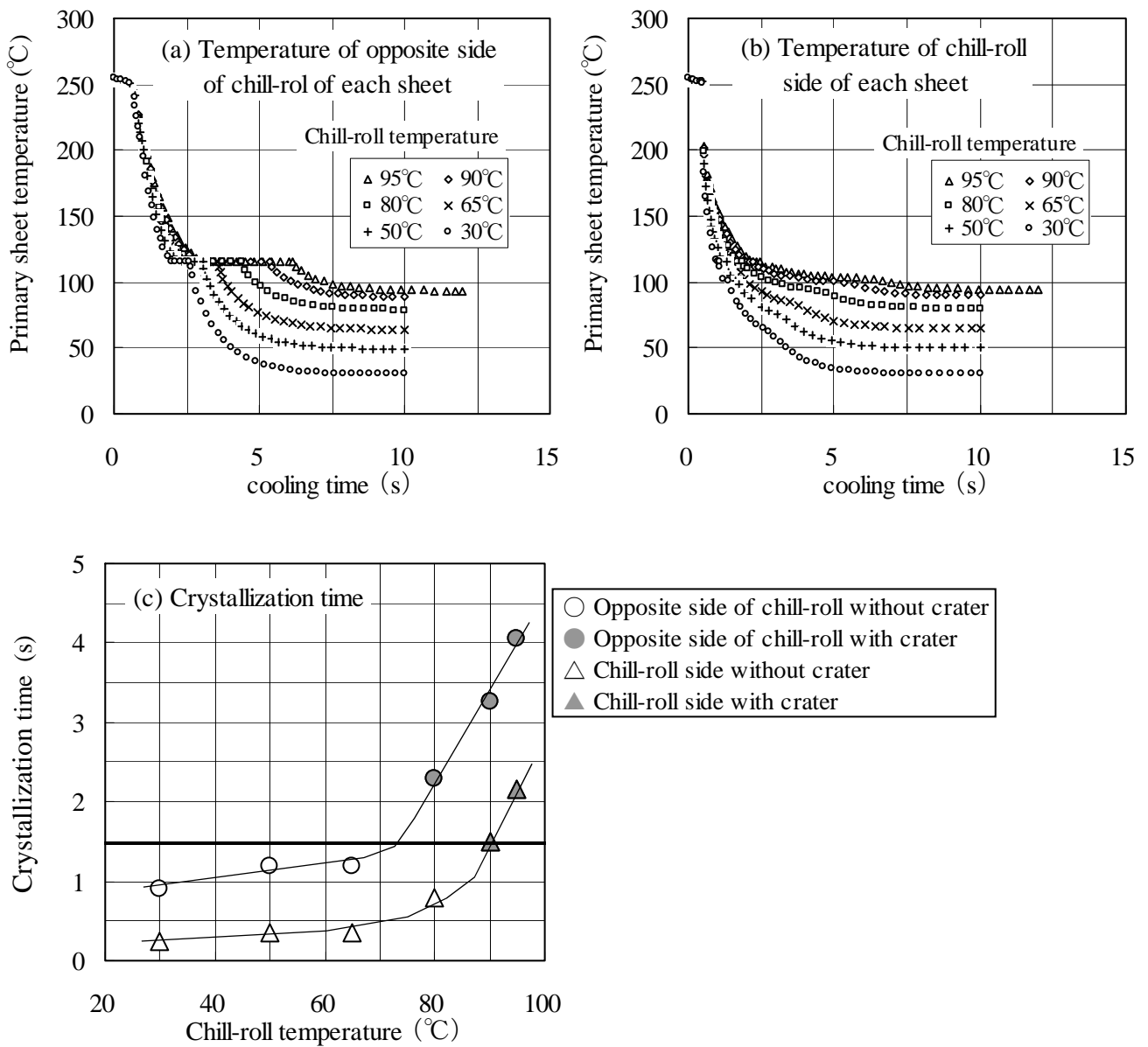


Fig.14 Calculated results of temperature of PP sheets with different chill-roll temperatures (Conditions: Die temperature; 250°C, Thickness of PP sheets; 300 μ m, Stretching temperature; 159°C, Stretching ratio; MD/TD=5/7)

Table 3 Changes of spherulite size during stretching to the machine direction (Unit: μm)

Sheet	Stretching ratio (-)	
	1	2
A80-100	4.9	5.6
A30-300	6.5	9.8

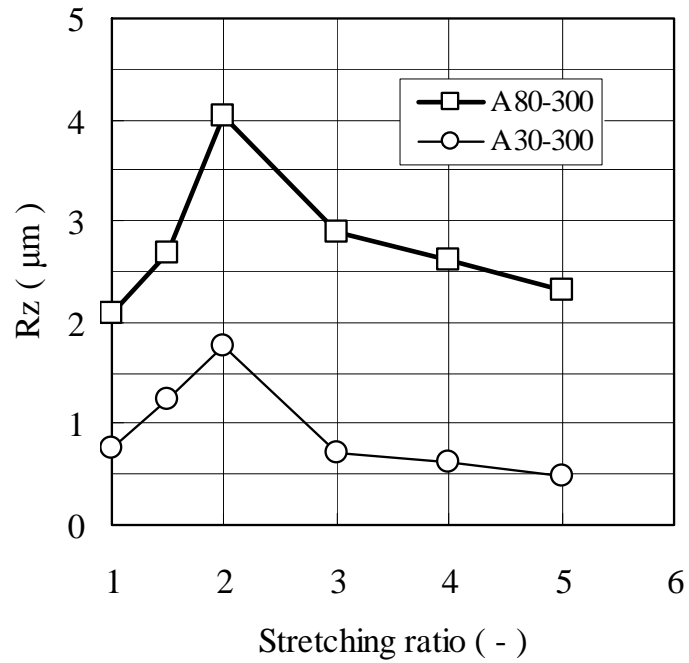


Fig.15 Rz of BOPP films stretched by opt-rheometer obtained from PP sheets with different chill-roll temperatures

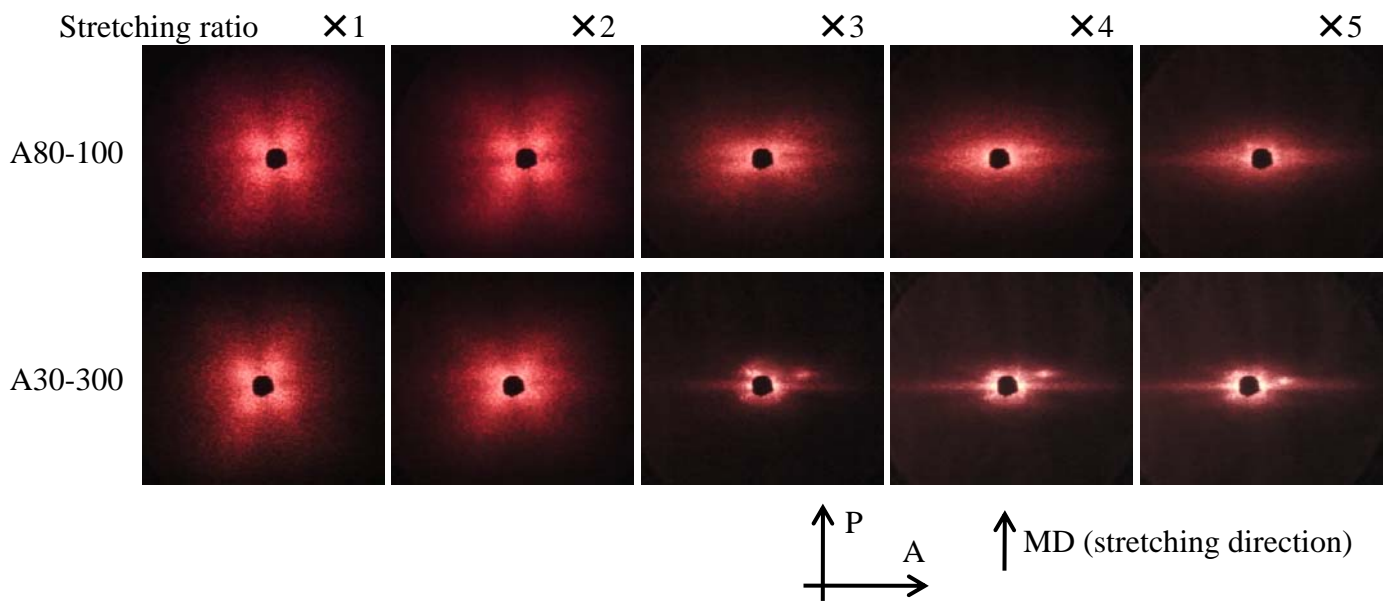


Fig.16 Light scattering patterns stretched by opt-rheometer obtained from PP sheets with different chill-roll temperatures (P: Polarizer, A: Analyzer)